Microscopic and Macroscopic Signatures of Antiferromagnetic Domain Walls

R. Jaramillo,[1] T. F. Rosenbaum,[1,*] E. D. Isaacs,[2] O. G. Shpyrko,[2] P. G. Evans,[3] G. Aeppli,[4] and Z. Cai[5]

[1]*The James Franck Institute and Department of Physics, The University of Chicago, Chicago, Illinois 60637, USA*
[2]*Center for Nanoscale Materials, Argonne National Laboratory, Argonne, Illinois 60439, USA*
[3]*Department of Materials Science and Engineering, University of Wisconsin, Madison, Wisconsin 53706, USA*
[4]*London Centre for Nanotechnology and Department of Physics and Astronomy, UCL, London, WC1E 6BT, United Kingdom*
[5]*Advanced Photon Source, Argonne National Laboratory, Argonne, Illinois 60439, USA*

Magnetotransport measurements on small single crystals of Cr, the elemental antiferromagnet, reveal the hysteretic thermodynamics of the domain structure. The temperature dependence of the transport coefficients is directly correlated with the real-space evolution of the domain configuration as recorded by x-ray microprobe imaging, revealing the effect of antiferromagnetic domain walls on electron transport. A single antiferromagnetic domain wall interface resistance is deduced to be of order 5×10^{-5} $\mu\Omega$ cm^2 at a temperature of 100 K.

Magnetic domains constitute the internal architecture of a host of technologically interesting materials. How ferromagnetic domains form, move, and scatter electrons lies at the heart of items from electrical motors and transformers to data storage devices [1]. In an ordinary ferromagnet (FM), a domain is characterized by a single vector, namely, its magnetization. Antiferromagnets (AF) typically are characterized by multiple vectors corresponding to the local magnetization and how it evolves with position, and offer new and expanded microscopic architectures for exploitation. However, with neither a net magnetic moment nor long wavelength features, antiferromagnetic domains have resisted the detailed characterization that underpins the applications prevalent for ferromagnetic domains.

The field has grown in recent years, with an increasing number of studies focused on antiferromagnetic domain imaging [2–4] and an improved understanding of the microscopic details of the exchange-bias effect in magnetic microstructures [2]. Despite this progress, little attention has been devoted to the transport properties of AF domains and domain walls themselves. As the ability to craft device features progresses to ever smaller dimensions, and hybrid devices mixing ferromagnetic and antiferromagnetic components proliferate, the need to understand the effects on transport of antiferromagnetic domain structure on the microscale, and domain walls on the nanoscale, becomes increasingly acute.

We present here a combined electrical transport and x-ray microprobe imaging study of a model AF. We show that magnetotransport measurements on small single crystals of Cr, the elemental spin-density-wave AF, are highly sensitive to the domain structure, and we directly correlate the temperature-dependent and hysteretic behavior of the transport coefficients with the real-space evolution of the domain structure. Combining the x-ray images with the measured anisotropic resistivity yields a quantita-tive estimate of the electrical resistance of a single antiferromagnetic domain wall.

The incommensurate spin-density wave (SDW) in chromium is an antiferromagnetic state that is caused by a nesting instability of the paramagnetic Fermi surface [5,6]. The SDW modulation vector **Q** is selected by the nesting condition and may lie along any of the cubic crystallographic axes, leading to so-called "*Q* domains." Between the Néel ordering temperature $T_N = 311$ K and the spin-flop temperature $T_{\mathrm{SF}} = 123$ K, the SDW is in the transverse phase ($\mathbf{S} \perp \mathbf{Q}$) and the spins preferentially lie along either cubic axis perpendicular to **Q**, leading to so-called "*S* domains." Below T_{SF} the SDW is longitudinal ($\mathbf{S} \parallel \mathbf{Q}$). This multiple degeneracy, threefold for the direction of **Q** and twofold for the direction of **S** in the transverse phase, leads to a rich variety of domain interfaces involving rotations of both the Fermi surface and the spin polarization, with great potential for modulating spin and charge transport.

The nested portions of Fermi surface are eliminated in the magnetic state by the formation of an energy gap; the non-nested portions remain ungapped, and are responsible for the metallic behavior for $T < T_N$. The partially gapped nature of the SDW state has complicated anisotropic effects on transport, which can be modeled semiquantitatively. Results for the resistivity tensor are available in the literature [7,8], derived from samples that have been specially prepared in a single-*Q*-domain state, with a resistivity anisotropy of approximately 10% at low temperature. However, akin to the state of play for ferromagnets in the 1960s [9,10], little is known for antiferromagnets about the effect of domain walls on the electrical transport.

We present in Fig. 1 a schematic AF domain structure. The domain wall is defined by two potentially independent rotations $\hat{\eta}_S/R$ and $\hat{\eta}_Q/R$ of the spin polarization and modulation vectors, respectively, where R represents the wall thickness. This compares to a FM where the domain
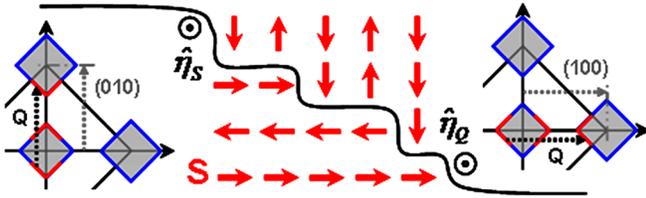
FIG. 1 (color online).   Schematic AF domain structure in Cr.
Only one of the two possible spin polarizations **S** is illustrated
for each Q domain; hence we show only one of the four types of
boundary that are possible between this pair of Q vectors. The
rotations $\hat{\eta}_S$ and $\hat{\eta}_Q$ (defined in the text) that characterize the
domain wall are collinear for this particular domain wall real-
ization. In reciprocal space the gapped and ungapped Fermi
surfaces are shown in red and blue, respectively. The electron
Fermi surface centered at the middle of the Brillouin zone and
the hole surface centered at the corner of the zone are connected
by the nesting vector **Q**. Only the magnetic bands are shown for
clarity.

FIG. 2 (color online).   (a) Superposition of actual sample wired
for electrical measurements with a typical Q-domain image to
scale, permitting direct comparison of the length scales involved.
Domain wall motion, such as that seen in Figs. 3 and 4, is
significant on the length scale of the current paths. (b) Difference
between the longitudinal resistivities $\Delta\rho \equiv \rho_{xx} - \rho_{yy}$ showing
thermal hysteresis and clear evidence for domain rearrange-
ment with changes in temperature. Residual ($T = 10$ K) and
room temperature ($T = 300$ K) resistivities are 0.24 and
11.70 $\mu\Omega$ cm, respectively. The (x, y) coordinates are defined
by the sample geometry.

wall simply is defined by a single rotation $\hat{\eta}_S/R$. The
electronic properties of the domain wall are dominated
by the ability of the electrons to scatter between domains
with differing Fermi surfaces, and this is largely depen-
dent on the relative extents of the domain wall R and the
conventional electron mean free path l. For domain walls
in a conventional FM such as Co, $R/l \gg 1$, with the re-
sult that domain wall interface resistances are small
($\sim 10^{-7}$ $\mu\Omega$ cm^2) [11]. For $R/l \lesssim 1$, quantum effects be-
come important and in materials with sharp domain wall
features the resulting tunneling magnetoresistances can be
much larger ($\sim 10^{-6}$–10^{-5} $\mu\Omega$ cm^2) [12]. At Q-domain
walls in Cr there is an abrupt, several lattice-constants wide
[13,14] range over which the anisotropic gap in the Fermi
surface rotates by 90° from one of the cubic axes to
another; see the band structure schematics in Fig. 1, with
the gapped portions of Fermi surface displayed in red. This
is accompanied by the observed 90° rotation in the spin-
density, charge-density, and lattice strain modulation
[3,14]. This means that when electrons flow across a
domain wall they move from an ungapped metallic Fermi
surface to one that is gapped and insulating. The condition
$R/l \sim 1$ is satisfied in Cr, where both quantities are on the
order of a few nm [14]. Q-domain walls, therefore, may be
significant charge- (and spin-) dependent scatterers.

We prepared three crystals measuring $(195 \times 180 \times
45)$ μm^3, $(460 \times 475 \times 60)$ μm^3, and $(675 \times 695 \times
80)$ μm^3 for transport measurements, guided by the work
of Evans *et al.* [3] who showed that the length scale of the
Q domains is tens of microns on a side, with S domains
somewhat smaller. Our intent was to measure samples
small enough so that the movement of a few domain walls
would cause a measurable change in the resistivity [see
Fig. 2(a)], but large enough to remain fully in the bulk
regime. All samples were oriented Cr single crystals cut
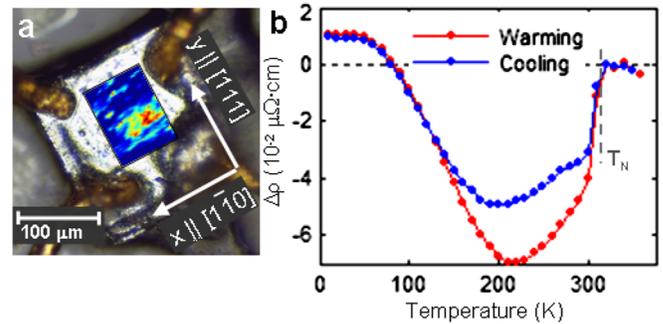along the noncubic $(1\bar{1}0)$, (111), and $(\bar{1}\bar{1}2)$ planes, pol-

ished to an optical finish, and etched to reduce domain
pinning by surface anisotropy [14], surface roughness, and
crystallographic strain. The full resistivity tensor in the
plane of the measurement was measured in the van der
Pauw configuration [15]. All temperature changes were
performed in zero-field to avoid field-induced biasing ef-
fects. Magnetic field measurements were in the linear
regime with $H \leq 0.5$ T. In order to make connections
between the bulk transport measurements and the under-
lying microscopic physics, we used the x-ray microprobe
beam line 2ID-D at the Advanced Photon Source to image
the AF domain structure of a crystal from the same wafer.
A submicron focused beam is produced at the sample face
by an x-ray Fresnel zone plate and is diffracted from one of
the order parameters, either the SDW or its second har-
monic charge-density wave. The sample is rastered to
create a two-dimensional intensity map of the order pa-
rameter in question [3].

The results of our combined transport and imaging study
are summarized in Figs. 2–4. We plot in Fig. 2(b) the
difference between the zero-field longitudinal resistivities
in the sample plane for both warming and cooling. These
differential data exhibit a pronounced thermal hysteresis
(large compared to that present in the individual longitu-
dinal resistivities). Particularly striking is the way in which
$\Delta\rho \equiv \rho_{xx} - \rho_{yy}$ suggests a shifting domain configuration
with temperature, with a clear onset just below T_N. A fixed
configuration could not produce the observed behavior, in
particular, the change of sign below 100 K and the thermal
hysteresis. Shifts in the domain configuration can be
thought of as local rotations of the anisotropic resistivity
tensor, and are easily visible in our data due to the small

number of domains encountered by a given current path
[Fig. 2(a)].

We find thermal hysteresis in all of the measured resis-
tivity components, but the effect is largest in the Hall
coefficient. We present this data in Figs. 3 and 4, along
with microprobe Q-domain images taken within similar
thermal loops and mapped onto the transport results. The
Hall hysteresis loop is robust, repeating over many thermal
cycles spanning hundreds of hours. The lower and upper
temperatures that define the hysteresis are 75 ± 15 K and
250 ± 15 K. The upper bound of our hysteresis loop cor-
responds to the temperature at which Q-domain fluc-
tuations are no longer detectable in electrical noise mea-
surements [16]. There is no signature of the spin-flop
transition in the transport data, pointing to the Q domains
rather than the S domains as the source of hysteretic
behavior. Measurements using thermal equilibration times
differing by more than an order of magnitude did not affect
the observed response and we saw no evidence of glassy
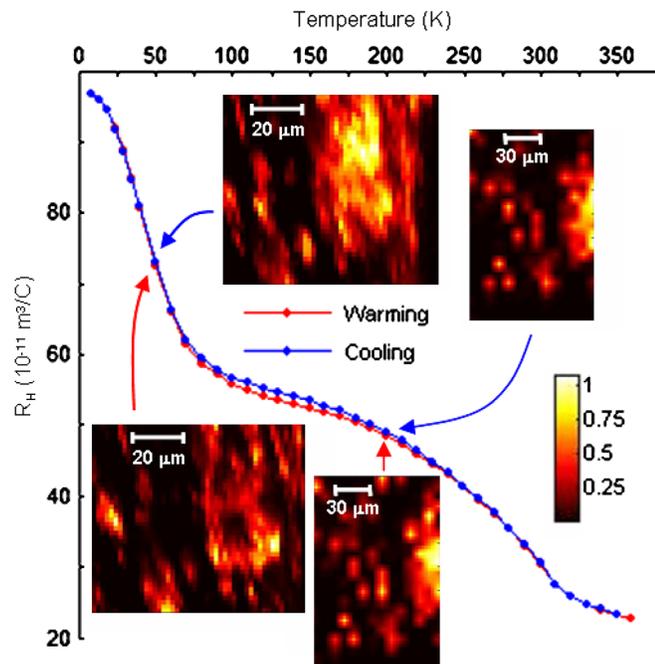relaxation or aging over hours.

FIG. 3 (color online). Thermal hysteresis of the Hall coeffi-
cient measured on a sub-mm Cr crystal. Images are maps of
microprobe diffraction intensity from one of three Q-domain
types; diffraction is from the charge-density wave satellite at (0,
0, $2 - 2\delta$), and therefore is sensitive only to domains with **Q** ∥
[001]. Beam spot size is 300×600 nm^2, sample face is (111),
x-ray energy is 11.6 keV, and the penetration length is ≈ 1.5 μm.
Images are taken at 50 K and 200 K within a thermal cycle
between 50 K and 300 K. Color bar indicates diffraction inten-
sity in counts/sec; multiplication factors of 2×10^4 and 10^4
should be used for the 50 K and 200 K images, respectively.
Images at the same T show the same sample area, but for
different T the areas imaged are different.

We plot our "master" Hall curve in Fig. 3. The response
follows the master curve regardless of whether the upper-
most temperature is above (as shown) or below (not shown)
T_N. Also presented in Fig. 3 are pairs of Q-domain images
taken at 50 K and at 200 K, near the edges of the measur-
able Hall hysteresis, as the system executed a round-trip
temperature cycle between 50 and 300 K. The domain
patterns on warming differ from those taken at the same
temperature on cooling, and the nature of these differences
provides insight into the physical mechanism underlying
the hysteresis in the electrical measurements. This is seen
most clearly in the two images taken at 50 K, a temperature
at which there is no hysteresis in the transport data.
Although the interior structures—the relative Q-domain
populations—change, it is apparent that most of the do-
main walls have returned to their same positions. This
effect may be quantified by comparing the changes in total
domain area and boundary length between pairs of images
taken at the same temperature. We define the extent of a
domain by the condition that the diffraction intensity be at
least half of the peak intensity measured at the domain
centers. Comparing the 50 K images, the volume occupa-
tion of the observable Q-domain type for this scattering
geometry has changed by $63 \pm 4\%$ on cooling as compared
to warming, but the change in total domain wall length is
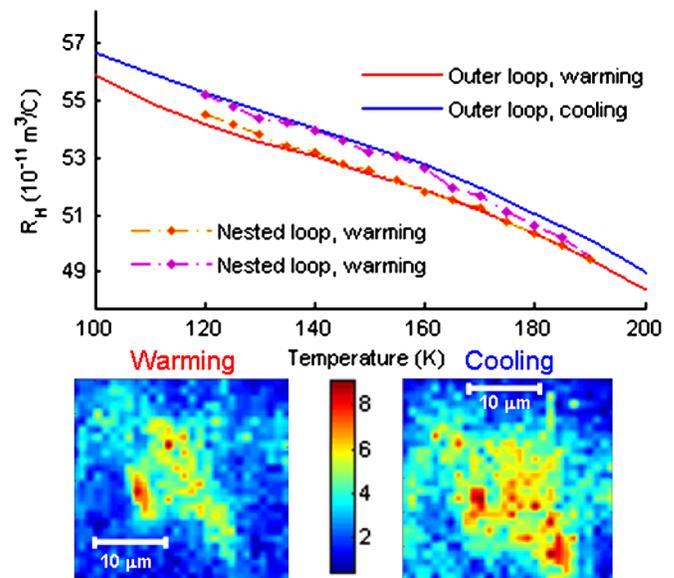only $4 \pm 3\%$. At 200 K, where the Hall effect still demon-

FIG. 4 (color online). Hall coefficient around a nested tem-
perature loop, showing persistence of hysteresis. Images are
maps of microprobe diffraction intensity from one Q-domain
type, taken at 110 K within a thermal cycle between 110 K and
170 K. Diffraction is from the magnetic satellite at (0, 1, δ);
below T_{SF} entire Q domains with **Q** ∥ [001] diffract at this
position [3]. Beam spot size is 300×600 nm^2, sample face is
(111), x-ray energy is 5.8 keV, and the penetration length
is ≈ 2 μm. Color bar indicates diffraction intensity in counts/
sec. Images show the same sample area.

P H Y S I C A L   R E V I E W   L E T T E R S

strates hysteresis, the volume occupation differs by $48 \pm 5\%$, and the domain wall length has changed by $42 \pm 6\%$. It is the spatial distribution of domain walls—not the fractional volume occupation of the Q domains—that appears to be most strongly selected by the pinning landscape and that correlates with the hysteresis in the Hall coefficient. We conclude that the domain walls themselves have a measurable effect on transport, and indeed have the dominant effect on the hysteresis.

Notably, the Hall response remains on the master curve as the system undergoes a series of nested thermal loops. The innermost such loop is shown in Fig. 4, presented alongside a pair of Q-domain images taken at 110 K within a similar thermal loop. We find that the Hall coefficient does not immediately snap to the cooling master curve after the turnaround point but does indeed find this master curve after a few downward steps in temperature; the system exhibits macroscopic return point memory [17]. Comparing the Q-domain images we see that there is significant hysteresis in the domain configuration, with a $182 \pm 80\%$ change in the volume occupation and an $81 \pm 50\%$ change in the total domain wall length (large error bars reflect the relatively poor counting statistics of magnetic x-ray diffraction). This large change is consistent with the Hall hysteresis, which reaches its maximum close to 110 K. These results suggest that the Hall coefficient is a particularly sensitive indicator of the underlying domain structure; this is mirrored by its sensitivity to the onset of the SDW itself at the quantum critical point [18].

The measured effect of domain motion on transport should decrease as the crystal size is increased since the longer current paths will see a greater number of domain walls and the effects of individual domain wall motion should then average out. This hypothesis is borne out by our measurements on the series of crystals of increasing size. As the sample volume increases by a factor of 8, and then by another factor of 3, the hysteresis in the Hall effect decreases by 35%: from a maximum of $2 \pm 0.2\%$ to $1.7 \pm 0.2\%$ to $1.3 \pm 0.2\%$.

We can estimate the resistance of a single domain wall by comparing results for the resistivity anisotropy in single-Q samples with data taken on poly-Q samples. This works best for bulk crystals where many domains contribute to the scattering. Taking values from the literature [7], we solve for an effective domain wall contribution to the bulk resistivity that increases from of order 50 nΩ cm at 100 K to 130 nΩ cm at 200 K. However, bulk crystals do not permit a reliable estimate of the contributions of a single domain wall. In our crystals, where there are only a few domains and we are able to determine an average domain length scale (10 μm) from direct imaging, we can take the bulk results and deduce a single AF domain wall interface resistance of order 5×10^{-5} $\mu\Omega$ cm^2 at 100 K. This compares to the $R/l \sim 1$ limit in FM, an intuitive result given the abrupt transition from ungapped to gapped Fermi surfaces across an AF wall in Cr. A first principles theory of carrier scattering from AF domain walls, involving much bigger symmetry groups than the analogous theory introduced decades ago for FM Bloch walls [10], would be an especially useful development. Our work contributes to the nascent science of AF domain walls as elements in electronic devices, and is complementary to ongoing work on FM domains and domain walls [1,2,19].

*Electronic address: t-rosenbaum@uchicago.edu
[1] L. Krusin-Elbaum *et al.*, Nature (London) **410**, 444 (2001); L. Zhang *et al.*, Science **298**, 805 (2002).
[2] F. Nolting *et al.*, Nature (London) **405**, 767 (2000); W. Kuch *et al.*, Nat. Mater. **5**, 128 (2006).
[3] P. G. Evans *et al.*, Science **295**, 1042 (2002); P. G. Evans and E. D. Isaacs, J. Phys. D **39**, R245 (2006).
[4] J. W. Kim *et al.*, Appl. Phys. Lett. **87**, 202505 (2005).
[5] P. A. Fedders and P. C. Martin, Phys. Rev. **143**, 245 (1966).
[6] S. A. Werner, A. Arrott, and H. Kendrick, Phys. Rev. **155**, 528 (1967).
[7] A. L. Trego and A. R. Mackintosh, Phys. Rev. **166**, 495 (1968); W. B. Muir and J. O. Ström-Olsen, Phys. Rev. B **4**, 988 (1971).
[8] Y. Furuya, J. Phys. Soc. Jpn. **40**, 490 (1976).
[9] G. R. Taylor *et al.*, Phys. Rev. **165**, 621 (1968).
[10] G. G. Cabrera and L. M. Falicov, Phys. Status Solidi B **61**, 539 (1974).
[11] W. L. Lee, F. Q. Zhu, and C. L. Chien, Appl. Phys. Lett. **88**, 122505 (2006); M. Viret *et al.*, Phys. Rev. Lett. **85**, 3962 (2000).
[12] N. D. Mathur *et al.*, J. Appl. Phys. **86**, 6287 (1999); J. L. Prieto, M. G. Blamire, and J. E. Evetts, Phys. Rev. Lett. **90**, 027201 (2003).
[13] E. W. Fenton, Phys. Rev. Lett. **45**, 736 (1980).
[14] K. F. Braun *et al.*, Phys. Rev. Lett. **85**, 3500 (2000).
[15] H. C. Montgomery, J. Appl. Phys. **42**, 2971 (1971).
[16] R. P. Michel *et al.*, Phys. Rev. B **44**, 7413 (1991).
[17] M. S. Pierce *et al.*, Phys. Rev. Lett. **90**, 175502 (2003).
[18] A. Yeh *et al.*, Nature (London) **419**, 459 (2002).
[19] H. X. Tang *et al.*, Nature (London) **431**, 52 (2004); F. S. Bergeret, A. F. Volkov, and K. B. Efetov, Phys. Rev. B **66**, 184403 (2002).